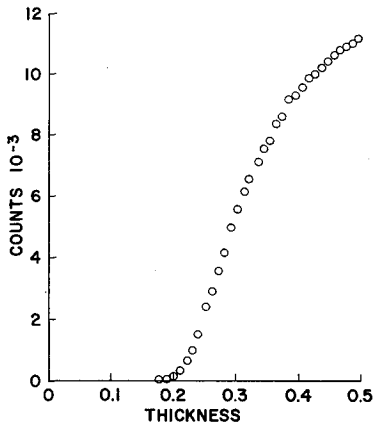

Fig. 1 Sensor accuracy: calibration curve of counts (second) vs plug thickness for graphite-phenolic plug with 1% dispersion of hafnium carbide.

the same for each sensor, then calibration curves obtained from one plug will hold for all the others. This fact was verified by chemical analyses and additional machining. A calibration curve was obtained by plotting the counts normalized to 100% vs the plug's length (Fig. 1). This type of calibration curve is the basis for interpretation of flight data.

To this point, it has been assumed the hafnium remains stationary until it is carried off in the char. In order to be assured that the hafnium did not diffuse throughout the material, a sensor plug contained in a model was exposed to a high-temperature air plasma. The conditions of the test were as follows: run time —10 sec, heat flux —1910 Btu/ft²-sec., cold wall; stagnation enthalpy —6020 Btu/#; surface temperature —5400°F. In an x-ray analysis of the plug before and after the test no diffusion or migration of the hafnium could be detected. The concept of radioactive nuclei being carried away by ablation decreasing the activity of a plug is straightforward enough, but to be useful, a suitable method of detecting such changes must be employed.

In the time schedule allotted to preparing this sensor concept for flight, it was necessary to make do with modifications of avaliable equipment rather than become involved with a large-scale development program for the detectors and signal processing electronics. The gamma radiation is detected by two Amperex Geiger-Muller tubes tied together so that their outputs add. A buffer amplifier reduces the effect of stray capacitance within the Geiger tube package, provides nearly ideal summing, and effectively isolates the tubes from effects of output cable capacitance and load impedance. The output signal goes through a pulse shaping segment and is fed into a frequency to d.c. converter. The output from the converter is a signal in the range of 0–4 v sampled twenty times a second. This signal is fed into the telemetry system,

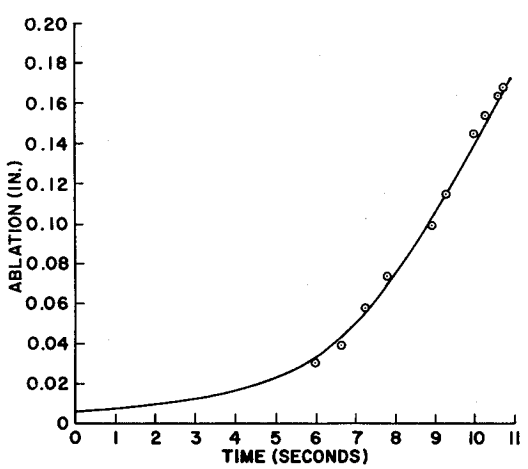

Fig. 2 In-flight ablation measurements from graphite-phenolic plug containing 1% hafnium carbide (irradiated).

which employs a pulse width modulation scheme. The telemetry signal is recorded by the ground tracking stations and the tapes are returned so that the data can be reduced.

The tapes are played back through an automatic decomutation system that produces a printout of the percent of full-scale signal vs time after liftoff. The data were analyzed in the following manner:

1) Examine the individual data points and delete those that exceed the average of the neighboring points by ±10%.

2) Average the time and percent signal for 1 sec (20 data points), reiterate every 0.2 sec.

3) Relate the averages obtained above to 100%. (The liftoff signal as a rule will not be quite 100% of full scale.)

4) Correlate these percentages to the calibration of the individual telemetry channel.

5) Obtain thickness values corresponding to percentages from the thickness/% signal calibration curve and subtract this thickness from the 100% value to obtain ablation.

6) Plot ablation vs time after liftoff. Figure 2 is a typical ablation time history of a point on a heat shield during reentry, as measured by the dispersed radioactive ablation sensor.

Conclusions

The development of the sensor has concentrated on reinforced phenolic materials but is applicable to all ablation materials. Sensor prototypes containing a dispersion of hafnium carbide have been successfully fabricated for various refractory reinforced phenolics, polyfluroethylene, the pyrolytic graphites, and elastomeric materials. An investigation of the natural extension of these sensors to measure degradation has begun and a dual system sensor employing pulse height discrimination to measure ablation and degradation is feasible.

Nonhomogeneous Impact Attenuator for Spherical Landing Capsule

GERALD J. CLOUTIER*
Sylvania Electronic Systems—East, Waltham, Mass.

Nomenclature

G = acceleration, g's
n = exponent (measure of nonhomogeneity)
R = radius, ft; R_2 = outside radius, ft
S = crushing stress, lb/ft²
m = mass, slug (lb-sec²/ft)
t = thickness, ft
u_m = dimensionless coordinate $\equiv 1 - t/R_2$
v_0 = impact velocity, fps
w = weight, lb
y = coordinate, ft; $\ddot{y}$ = acceleration, ft/sec²
α, β = constants
ϵ = usable strain, in./in.
ρ = mass density, slug/ft³ (lb-sec²/ft⁴)

Subscripts

i, c, m = instrument package, crushable material, and maximum, respectively

Introduction

SPHERICAL landing capsules protected omnidirectionally by crushable material have been designed for Ranger missions to the moon and suggested for precursor probes to

Received April 10, 1967. [1.02, 6.08, 6.13]
* Advanced Development Engineer, Satellite Antenna Department. Member AIAA.

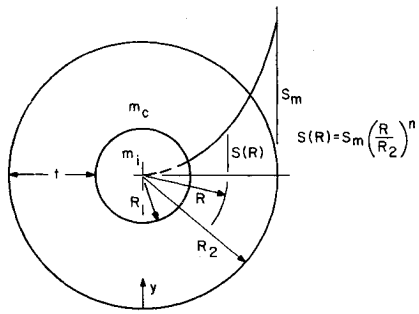

Fig. 1 Variable crushing-stress parameters.

planets. As information on the behavior of these materials is accumulated and techniques for treating the impact dynamics are improved, the probe designs are becoming more sophisticated.[1] This note investigates the possible benefits of nonhomogeneous crushup that is spherically symmetric and isotropic (so that the stress is a function of the radial coordinate only) and is made by laying up successive spherical shells of materials with different crushing stresses. Cundall[1] studies the use of layers of balsa woods of different densities; the sample case treated herein involves the use of honeycombs.

Basic Derivation

Most of the pertinent parameters are illustrated in Fig. 1. The expressions for acceleration at any time during the impact and for the initial impact velocity were derived in Ref. 2 for the case where the crushing stress of the attenuator is a variable (but spherically symmetric). Those equations can be put into the form

$$\ddot{y} = \left(\frac{2\pi}{m_i + m_c}\right) \int_{R_2 - y/\epsilon}^{R_2} RS(R)dR \tag{1}$$

$$v_0^2 = \left(\frac{4\pi}{m_i + m_c}\right) \int_0^{y_m} \int_{R_2 - y/\epsilon}^{R_2} RS(R)dRdy \tag{2}$$

where ϵ is the so-called "usable strain" of the material; its inclusion in the equations accounts for the fact that the material does not crush completely. To obtain some idea of how the stress variation affects the results, a particular function $S(R)$ was chosen:

$$S(R) = S_m(R/R)^n \tag{3}$$

A more complicated expression could have been chosen, such as a polynomial in R, but the foregoing form permits all relevant expressions to be integrated (particularly the relation for crushable material mass which is derived below). Further, it allows us to use the single parameter n as a measure of the "degree of nonhomogeneity" in parametric studies. Substituting Eq. (3) into (1) and (2) yields, with $y_m = \epsilon t$,

$$\ddot{y} = [2\pi S_m R_2^2/(n+2)(m_i + m_g)] \times [1 - (1 - y/\epsilon R_2)^{n+2}] \tag{4}$$

$$v_0^2 = 2\epsilon R_2 \xi \{t/R_2 - [1 - (1 - t/R_2)^{n+3}]/(n+3)\} \tag{5}$$

where $\xi \equiv 2\pi S_m R_2^2/(n+2)(m_i + m_c)$. Equation (4) is plotted on Fig. 2 and illustrates that as the exponent n is increased, the deceleration curve approaches the ideal, constant deceleration curve. Thus, this type of nonhomogeneous construction ought to yield a more efficient impact attenuator, which conclusion is borne out by the sample problem discussed below. Defining $u_m \equiv 1 - t/R_2$,

$$\ddot{y}_m = [2\pi S_m R_2^2/(n+2)(m_i + m_c)][1 - u_m{}^{n+2}] \tag{6}$$

$$v_0^2 = [4\pi\epsilon S_m R_2^3/(n+2)(m_i + m_c)][1 - u_m - (1 - u_m{}^{n+3})/(n+3)] \tag{7}$$

Division of Eq. (7) by Eq. (6) gives a kinematic equation

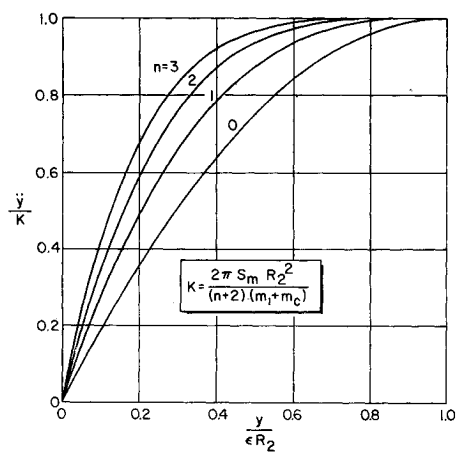

Fig. 2 Graph of normalized acceleration vs stroke.

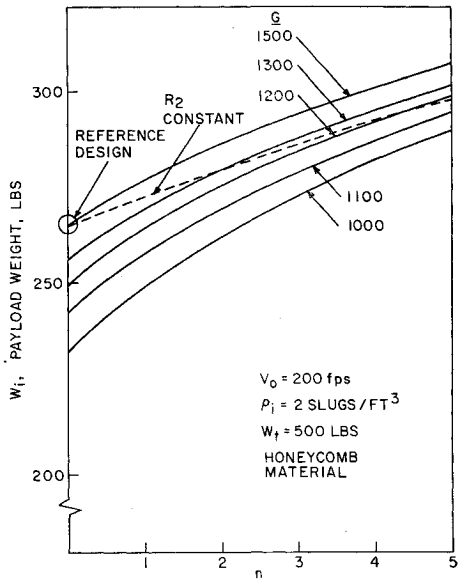

Fig. 3 Graph of payload weight vs degree of nonhomogeneity.

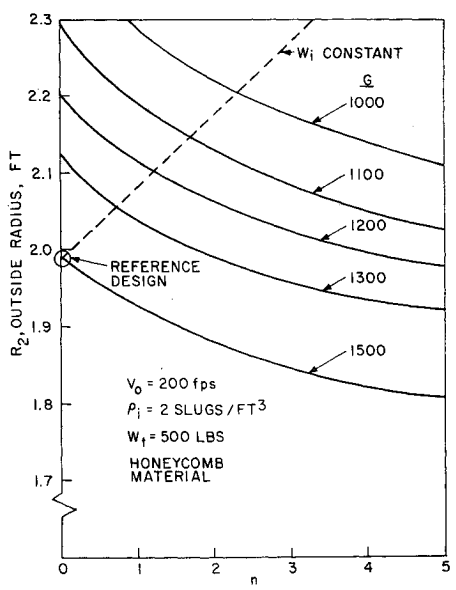

Fig. 4 Graph of outside radius vs degree of nonhomogeneity.

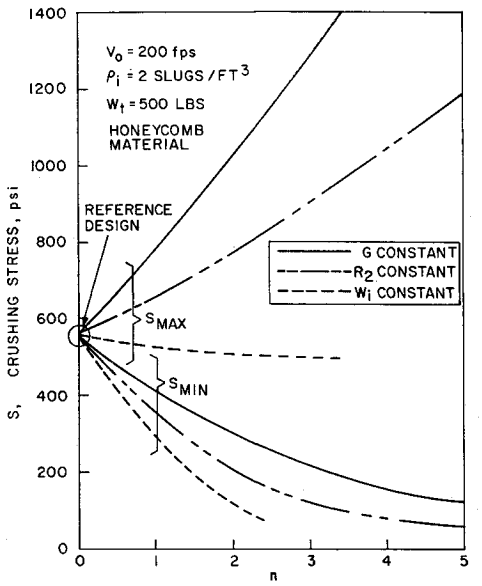

Fig. 5 Graph of maximum and minimum crushing stress vs degree of nonhomogeneity.

relating velocity, acceleration, and stroke:

$$v_0^2/\epsilon\ddot{y}_m = 2R_2[1 - u_m - (1 - u_m{}^{n+3})/(n + 3)]/(1 - u_m{}^{n+2}) \quad (8)$$

Now, assuming that the lander is a complete sphere, the mass of the crushable material can be calculated. The incremental mass of a spherical shell of thickness dR is

$$dm_c = 4\pi\rho_c R^2 dR$$

If a single type of crushable material is used, such as aluminum honeycomb, it is possible to fit a curve to the plot of material properties. It has been found, in fact, that a curve of the form $\rho_c = S^\beta/\alpha$ can be fit to most of the materials of interest.[2] Using this equation, the total crush-up mass is

$$m_c = 4\pi\rho_{cm}R_2{}^3(1 - u_m{}^{\beta n+3})/(\beta n + 3) \quad (9)$$

where ρ_{cm} is the mass density corresponding to the maximum crushing stress S_m. Equations (7–9), together with an equation for payload mass,

$$m_i = \tfrac{4}{3}\pi\rho_i R_1{}^3 = \tfrac{4}{3}\pi\rho_i R_2{}^3 u_m{}^3 \quad (10)$$

form the basis for parametric studies of the effect of using nonhomogeneous design of crushable-material impact absorbers.

Example and Conclusions

An impact velocity of 200 fps, a payload packing density of 2 slug/ft^3, and a total landed weight of 500 lb are assumed. A honeycomb class of crushable material (either plastic or metal) is specified, for which $\rho_c = S^{0.554}/2080$, and $\epsilon = 0.75$. The reference design is a 1500-g impact with homogeneous material. The results of parametric studies using a digital computer program of the foregoing equations are summarized in Figs. 3–5.

If the deceleration level is held constant at 1500 g's, then increasing n brings about some increase in payload w_i and a significant reduction in outside radius R_2. Although the range of crushing stress is quite wide (Fig. 5) the values are achievable with current materials. If, instead, w_i is held fixed while n is increased, a substantial reduction in the g level results, but R_2 increases significantly because more ow-density, inefficient honeycomb material is being used. Reference 1 indicates, that for this case using balsa wood, here is little change in R_2.) Further, the minimum crushing tress required rapidly decreases to a point where it is unfeasible. A compromise between these two cases can be obtained by holding R_2 fixed; then G decreases, w_i increases, and the variations required in S are moderate.

The main problem in implementing this technique would be avoiding the "cannon-ball" effect, where the payload starts to move independently and to crush the energy-absorption material internally.[1,2] If tension ties between the payload and the crushable material are sufficiently strong to prevent this effect, then this technique would allow significant improvements in the design of hard-landing, omnidirectionally protected planetary probes.

References

[1] Cundall, D. R., "Balsa-wood impact limiters for hard landing on the surface of Mars," *AIAA/AAS Stepping Stones to Mars Meeting* (American Institute of Aeronautics and Astronautics, New York, 1966), pp. 302–308.

[2] Cloutier, G. J., "Landing impact energy absorption using anisotropic crushable materials," J. Spacecraft Rockets **3**, 1755–1761 (1966).

Potential of Low-Power Thermionic Devices for Terrestrial Applications

F. T. Princiotta* and T. S. Bustard†
Hittman Associates Inc., Baltimore, Md.

To date, the bulk of thermionic systems development effort has been related to space utilization. At a lower level of effort has been terrestrial thermionic development, and almost all of this has related to design of hydrocarbon-fired thermionic devices. Only a very small effort has been expended on development of isotope-fueled terrestrial thermionic generators. This note presents an evaluation of the potential of such nuclear systems.

The main development problem associated with hydrocarbon-fired generators has been the maintenance of diode vacuum integrity in the hot gas environment associated with hydrocarbon combustion. This problem is aggravated by the high temperatures associated with hydrocarbon thermionic conversion (1400°C emitter temperature), since gas permeation increases exponentially with temperature. Another major problem area is the development of an efficient regenerative burner at thermionic temperatures, particularly for nongaseous hydrocarbons, to increase generator thermal efficiency.

Isotope thermionic generators would be heavier, bulkier, and less mobile, relative to hydrocarbon systems, largely due to the substantial amount of biological shielding required. However, such units should be capable of longer term, unattended operation due to the long periods between fuelings associated with isotope heat sources such as Sr-90 and Co-60 with their half-lives of 27.7 and 5.25 yr, respectively. In addition, such units could be effectively utilized for undersea applications.

Isotope Selection

Thermionic devices require a high emitter temperature with a correspondingly high-thermal-flux requirement (20–60 w/cm^2). Thus a high-power-density fuel is desired, and only

Presented as Paper 66-1007 at the AIAA Third Annual Meeting, Boston, Mass., November 29–December 2, 1966; submitted December 6, 1966; revision received April 6, 1967. [5.02, 5.08]

* Senior Engineer.

† Manager, Isotopic Power and Radiation Applications Section.